

1

2

Journal of Geophysical Research: Planets

3

Supporting Information for

4

Properties of Lunar Regolith on the Moon's Farside unveiled by Chang'E-4 Lunar Penetrating Radar

5

6

Zehua Dong^{1,2}, Guangyou Fang^{2,3,4*}, Bin Zhou^{2,4}, Di Zhao^{2,3}, Yunze Gao², and Yicai Ji²

7

¹School of Information and Electronics, Beijing Institute of Technology, Beijing 100081, China.

8

²Key Laboratory of Electromagnetic Radiation and Sensing Technology, Aerospace Information Research Institute, Chinese Academy of Sciences, Beijing 100190, China

9

10

³University of Chinese Academy of Science, Beijing 100149, China

11

⁴Greater Bay Area Research Institute of AIR-CAS, Huangpu, Guangzhou, China.

12

13

14

Contents of this file

15

16

Text S1 to S4

17

Figures S1 to S9

18

19

Introduction

20

- Text S1: Signal processing methods for LPR data;

21

- Text S2: Layer localization method for LPR data;

22

- Text S3: Estimation for dielectric properties of lunar regolith;

23

- Text S4: Estimation for permittivity of lunar subsurface materials;

24

- Figure S1: The raw LPR Channel-II data;

25

- Figure S2: The LPR Channel-II data after DC removing and background removing.;

26

- Figure S3: The radargram of processed LPR data;

27

- Figure S4: The frequency spectrum of LPR signal;

28

- Figure S5: The LPR Channel-II data after Amplitude Compensation;

- 29 • Figure S6: The schematic for the layer localization method;
- 30 • Figure S7: The model of subsurface layers in Li *et al.* (2020, *Sci. Adv.*);
- 31 • Figure S8: Mechanism of the hyperbolic fitting method;
- 32 • Figure S9: One trace of calibration signals of LPR Channel-II.

33 **Text S1. Signal processing methods for LPR data**

34 The transmitter of Chang'E-4 (CE-4) lunar penetrating radar (LPR) produces ultra-
35 wide band (UWB) carrier-free nanoseconds pulse and radiates UWB signals downward by
36 transmitting antenna. The signals would reflect and scatter when meeting buried objects
37 during propagation, such as interfaces between different medium, subsurface voids and
38 subsurface boulders. The time window and the sampling point of CE-4 LPR Channel-II
39 are 640 ns and 2048, respectively.

40 Considering the radar system noise and the out-of-band environment noise, the raw
41 LPR data are with low signal-to-noise ratio (SNR) (Fig. S1). Therefore, some processing
42 methods should be performed to improve the SNR of LPR data before further analysis.
43 Here, we employed direct-current (DC) removing, background removing, filtering and
44 amplitude compensation and so on, as usually used for ground penetrating radar data
45 on the earth applications (Jol, 2009; Dong et al., 2016).

46 1. Direct-current (DC) Removing

47 Direct-current (DC) component comes from the oscillation of low frequency during
48 the saturation recovery procedure of receiver. It should be removed before subsequent
49 processing because it doesn't indicate any useful information. The process of DC
50 removing is to slide a window from the beginning to the end of one trace, and then
51 compute the average within the window and subtract the mean value from center value
52 of the window, as shown in equation (S1).

$$53 \quad Y(n) = y_c - \frac{1}{N} \sum_1^N y(n) \quad (S1)$$

54 Where, y_c and $Y(n)$ represent the values of amplitude before and after processing,
55 respectively. $y(n)$ represents raw LPR data, N is the window length.

56 2. Background Removing

57 Background removing aims to eliminate the repetitive and successive interference at
58 the same time delay in every trace. Here we used it to remove the direct wave that
59 coupled from transmitting antenna to receiving antenna, so only the part before surface
60 echoes was processed. The processed amplitude could be derived as equation (S2).

61
$$x'(m, n) = x(m, n) - \frac{1}{N} \sum_{n=0}^{N-1} x(m, n) \quad (S2)$$

62 Where $x(m, n)$ is raw LPR data, $x'(m, n)$ is processed data, N is the trace number.
63 The LPR data after DC removing and background removing are shown in Fig. S2.

64 3. Amplitude Compensation

65 The LPR antenna could be approximated to an oscillating dipole that radiates
66 spherical waves. The amplitude of electromagnetic wave that propagates under the
67 ground suffers, therefore, a geometric attenuation due to the distribution of the energy
68 on the front of spherical wave. The amplitude $A(r)$ at the distance r is given as follows:

69
$$A(r) = G(r)A_0e^{-\alpha r} \quad (S3)$$

70 Where A_0 is the value of the initial amplitude transmitted from LPR antenna, α is
71 attenuation constant, $G(r)$ is the factor of geometrical spreading which can be derived
72 by equation (S4):

73
$$G(r) = \frac{1}{r} \quad (S4)$$

74 Therefore, the amplitude can be compensated by multiplying the LPR signals
75 by $1/G(r)$. The compensated data show more subsurface information because the
76 deeper signals are amplified, as shown in Fig. S3.

77 4. Filtering Processing

78 A filter in line with the characteristics of LPR data is an effective method to improve
79 the signal-to-noise ratio (SNR). The designed central frequency and bandwidth of CE-4
80 LPR Channel-II are 450MHz and 500MHz, respectively. Therefore, we chose a band-pass
81 filter with a pass band of 200-700MHz (Fig.S4).

82 From the above methods and procedures, the processed LPR data have improved
83 signal-to-noise ratio compared to the raw data (Fig.S5), which contributes to analyze the
84 subsurface geological structures and estimate the properties of lunar regolith.

85 **Text S2. Layer localization method for LPR data**

86 Because of the high pulse repetition frequency (PRF) of LPR and the low speed of
87 Yutu-2 roving, the LPR echoes of two adjacent traces from the same interface have

88 similar time delay and amplitude, namely, good correlation. Thus, we can take advantage
89 of the good correlation of two adjacent traces to localize the interface of subsurface
90 layers. However, the buried objects or other underground interference would influence
91 the effect of localization. As a result, we put forward a modified trace correlation method
92 in order to suppress interference and accurately extract subsurface layers, which includes
93 the following steps:

94 (1) Determination of initial values

95 Regard the first trace as reference trace and determine appropriate values for length
96 of reference window and search window, correlation threshold (T_C) and time threshold
97 (T_L) (T_C and T_L are empirical values), and then determine initial search point (P_1) by visual
98 inspection.

99 (2) Calculation of correlation

100 Take the next trace as target trace and calculate correlation between the signal in
101 reference window of reference trace and the signal in search window of target trace, and
102 then determine the maximum value of correlation (M_C) and corresponding point (P_2)
103 (Fig.S6).

104 (3) Determination of layer position

105 If $M_C > T_C$ and $|P_2 - P_1| < T_L$, then consider P_2 as the layer position of target trace,
106 also as the new search point, regard the target trace as new reference trace. If $M_C < T_C$,
107 or $M_C > T_C$ but $|P_2 - P_1| > T_L$, then consider the nearest extreme point from P_1 as the
108 layer position of target trace, but keep the preceding reference trace and search point.

109 (4) Implement step (2) and (3) to all the traces in order.

110 **Text S3. Estimation for dielectric properties of lunar regolith materials**

111 For LPR data interpretation purposes, the lunar subsurface geological structure at
112 CE-4 landing region could be modeled as a set of three planar layers (i.e., vacuum,
113 surface layer and subsurface layer) (Fig. 3). Each layer is assumed to be semi-infinite that
114 has a magnetic permeability equals to that of free space.

115 The reflection and transmission coefficients at each layer interface i can be described
 116 as follows:

$$117 \quad \gamma_i = \frac{\sqrt{\epsilon_{r,i}} - \sqrt{\epsilon_{r,i+1}}}{\sqrt{\epsilon_{r,i}} + \sqrt{\epsilon_{r,i+1}}} \quad (S5)$$

$$118 \quad \tau_i = \frac{2\sqrt{\epsilon_{r,i}}}{\sqrt{\epsilon_{r,i}} + \sqrt{\epsilon_{r,i+1}}} = 1 + \gamma_i \quad (S6)$$

119 The dielectric constant of the surface layer ($\epsilon_{r,1}$) can be derived from equation (S5):

$$120 \quad \epsilon_{r,1} = \epsilon_{r,0} \left(\frac{1-A_0}{1+A_0} \right)^2 \quad (S7)$$

121 Where $\epsilon_{r,0}$ is dielectric constant in vacuum. A_0 is signed relative reflection
 122 amplitudes which represents the ratio between the amplitudes of the surface reflection
 123 and the amplitude of the incident signal.

124 The relative amplitude of the reflected pulse at the interface between surface and
 125 subsurface A_1 can be given by:

$$126 \quad A_1 = (1 - \gamma_0^2) \gamma_1 e^{-\alpha d} \quad (S8)$$

127 where α is attenuation constant, d is thickness of surface layer. Approximate
 128 expression for α can be derived as:

$$129 \quad \alpha = \sigma_1 \eta_0 / 2 \sqrt{\epsilon_{r,1}} \quad (S9)$$

130 Where $\eta_0 = 120\pi$ is wave-impedance in free space. Replacing the reflection
 131 coefficient and the attenuation constant with their respective expressions yields the
 132 following equation:

$$133 \quad A_1 = (1 - A_0^2) \frac{\sqrt{\epsilon_{r,1}} - \sqrt{\epsilon_{r,2}}}{\sqrt{\epsilon_{r,1}} + \sqrt{\epsilon_{r,2}}} e^{-\eta_0 \frac{\sigma_1}{\sqrt{\epsilon_{r,1}}} d_1} \quad (S10)$$

134 The conductivity σ_1 can be found by transforming this equation, as given by
 135 equation (S11):

$$136 \quad \sigma_1 = \frac{\sqrt{\epsilon_{r,1}}}{d_1} \frac{1}{\eta_0} \log \left[\frac{1 - A_0^2 \frac{\sqrt{\epsilon_{r,1}} - \sqrt{\epsilon_{r,2}}}{\sqrt{\epsilon_{r,1}} + \sqrt{\epsilon_{r,2}}}}{-A_1 \frac{\sqrt{\epsilon_{r,1}} + \sqrt{\epsilon_{r,2}}}{\sqrt{\epsilon_{r,1}} + \sqrt{\epsilon_{r,2}}}} \right] \quad (S11)$$

137 As a result, the loss tangent and TiO₂+FeO content of lunar regolith can be derived
 138 subsequently.

139 Li *et al.* (2020) found that the bulk density is $\rho_{\text{bulk}} = 1.9 \text{ g/cm}^3$ (or 1.67 g/cm^3
 140 depending on their model) for a layer that is 6m thick. Hence, Li *et al.*'s dielectric
 141 constant of $\epsilon' = 3.5$ corresponds to the average ϵ'_r of the upper 6-m-thick regolith

142 material, as shown in Fig. S7. In this study, considering that the permittivity of lunar
 143 regolith increases rapidly at shallow depth, but increases more slowly at deeper depths,
 144 we assumed the average permittivity ($\epsilon_{r,1,average}$) of regolith materials as ~ 3.6 .

145 **Text S4. Estimation for permittivity of lunar subsurface materials**

146 LPR observes subsurface structures (such as boulders and interfaces) by detecting
 147 dielectric discontinuities. As the distance between the antenna and the subsurface object
 148 changes with the moving of Yutu-2 rover, single target buried in the subsurface
 149 produces parabolic-shaped diffraction (PSD) in the radar cross section.

150 Considering that rocks in the regolith mostly have irregular shapes and the effect of
 151 a rock's diameter will be reduced as the depth increases, we approximate the object as a
 152 point reflector in order to simplify the model. Fig. S8 demonstrates the mechanism of
 153 target detection for LPR. The propagating distance of electromagnetic (EM) wave from
 154 LPR to the subsurface object (L_1) and the minimum propagating distance when LPR is
 155 over the subsurface object (L) conform to Eq. (S12) based on the geometric relationship:

$$156 \quad L_1^2 - L^2 = D^2 \quad (S12)$$

157 Where D is the horizontal distance from LPR to the subsurface object, which can be
 158 derived according to the location of Yutu-2 rover. Moreover, L_1 and L could be described
 159 as Eq. (S13), respectively:

$$160 \quad L_1 = \frac{vt_1}{2}, \quad L = \frac{vt}{2} \quad (S13)$$

161 Where t_1 and t are the two-way propagating time corresponding to L_1 and L, v is
 162 the propagating velocity of EM wave.

163 The velocity of EM wave (v) is determined by the relative dielectric permittivity (ϵ_r)
 164 as:

$$165 \quad v = \frac{c}{\sqrt{\epsilon_r}} \quad (S14)$$

166 Where c is the speed of light in vacuum. Replacing the propagating distance in Eq.
 167 (S12) and the propagating velocity in Eq. (S13) with their respective expressions yields
 168 the following equation:

$$169 \quad \epsilon_r = \left(\left(c\sqrt{t_1^2 - t^2} \right) / 2D \right)^2 \quad (S15)$$

170 As a result, the relative dielectric permittivity of lunar subsurface materials can be
171 calculated with LPR data.

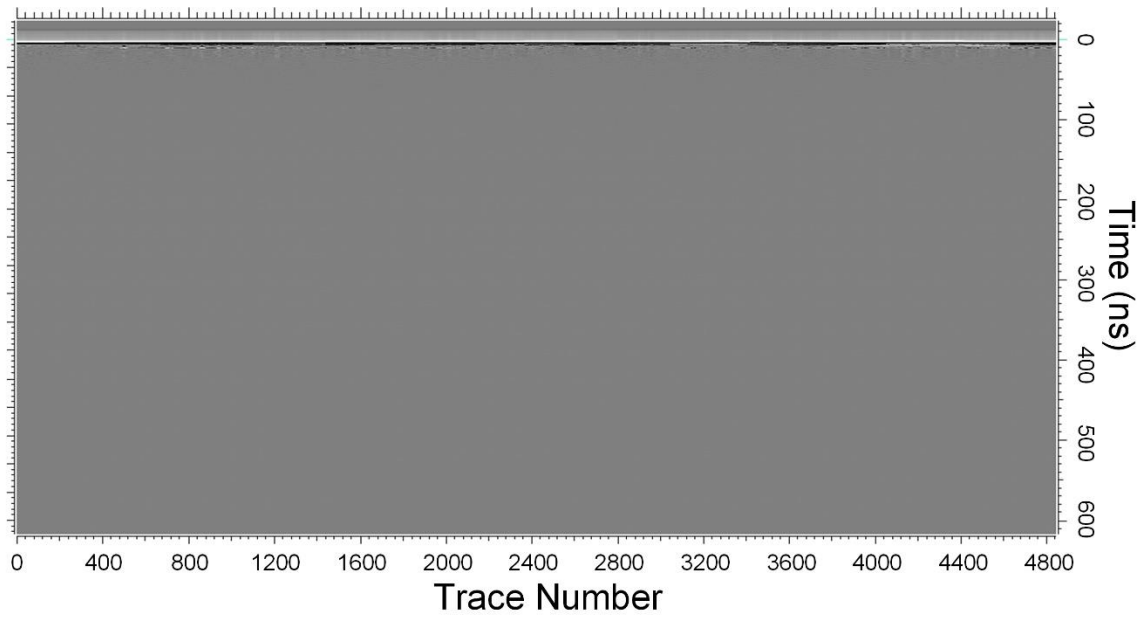


Figure S1. The raw LPR Channel-II data.

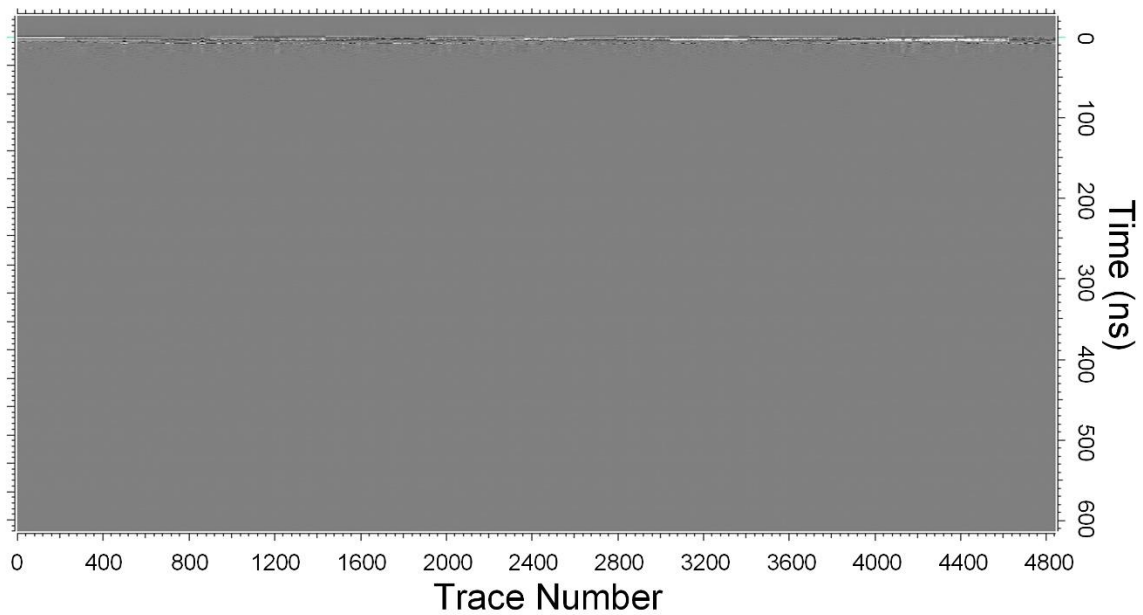


Figure S2. The LPR Channel-II data after DC removing and background removing.

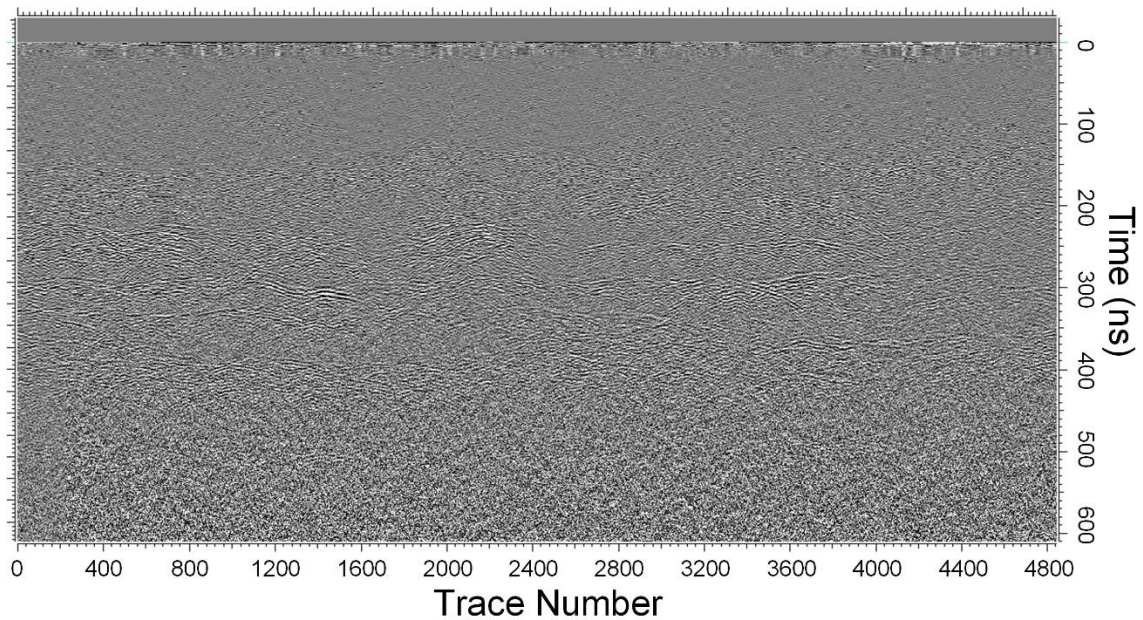


Figure S3. The LPR Channel-II data after Amplitude Compensation.

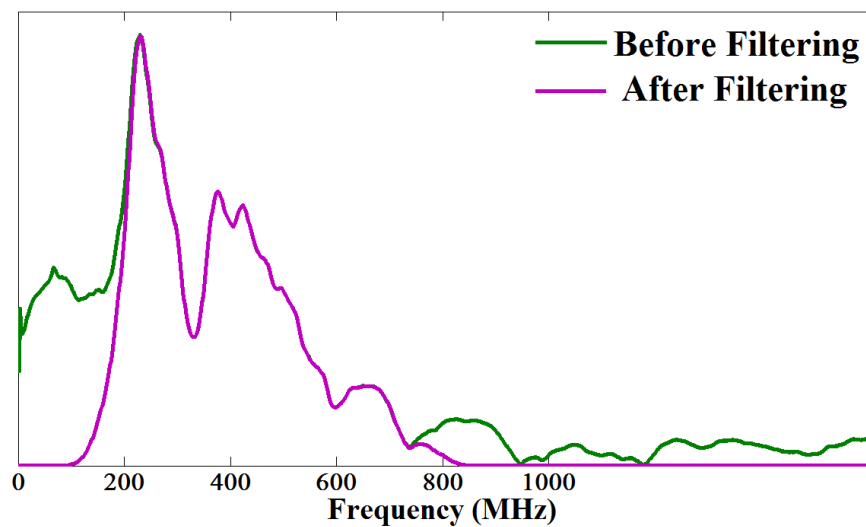


Figure S4. The frequency spectrum of LPR signal before (the green line) and after (the purple line) band-pass filtering.

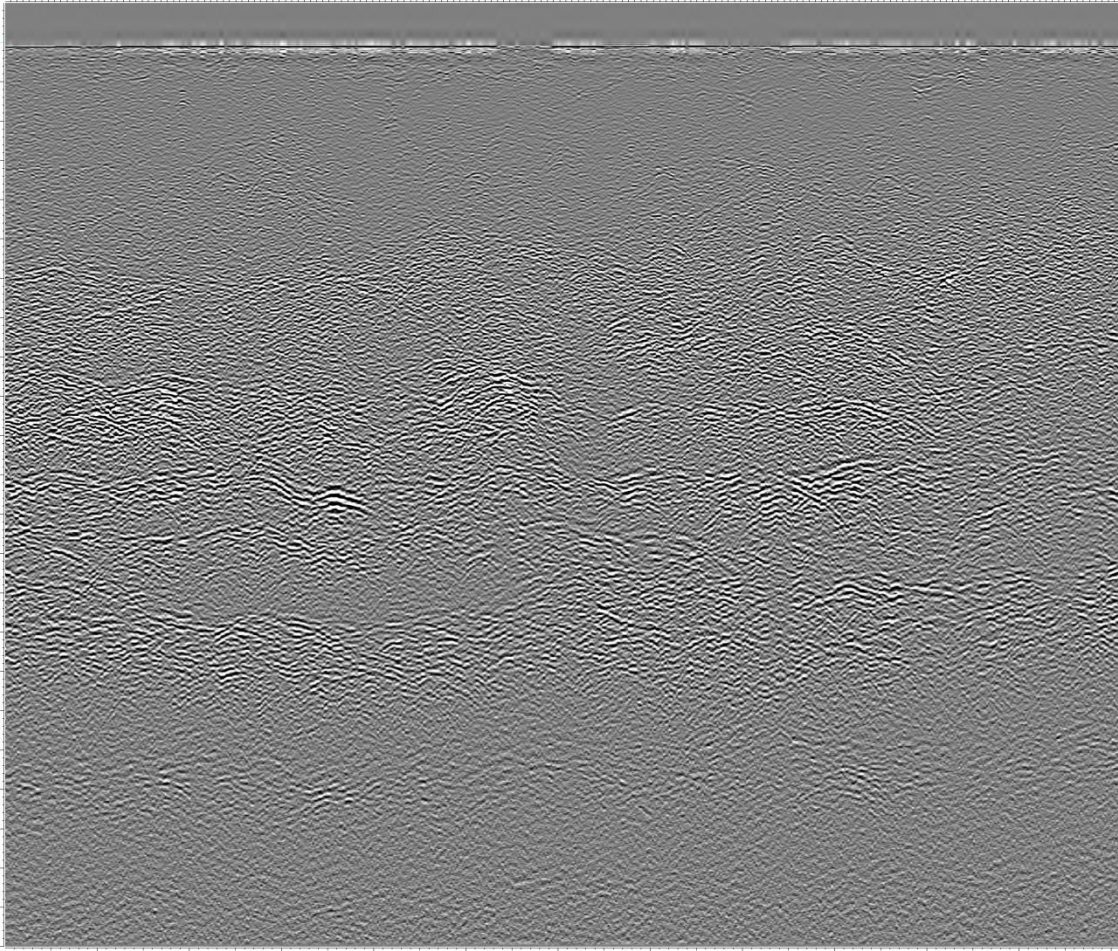


Figure S5. The radargram of processed LPR data after filtering.

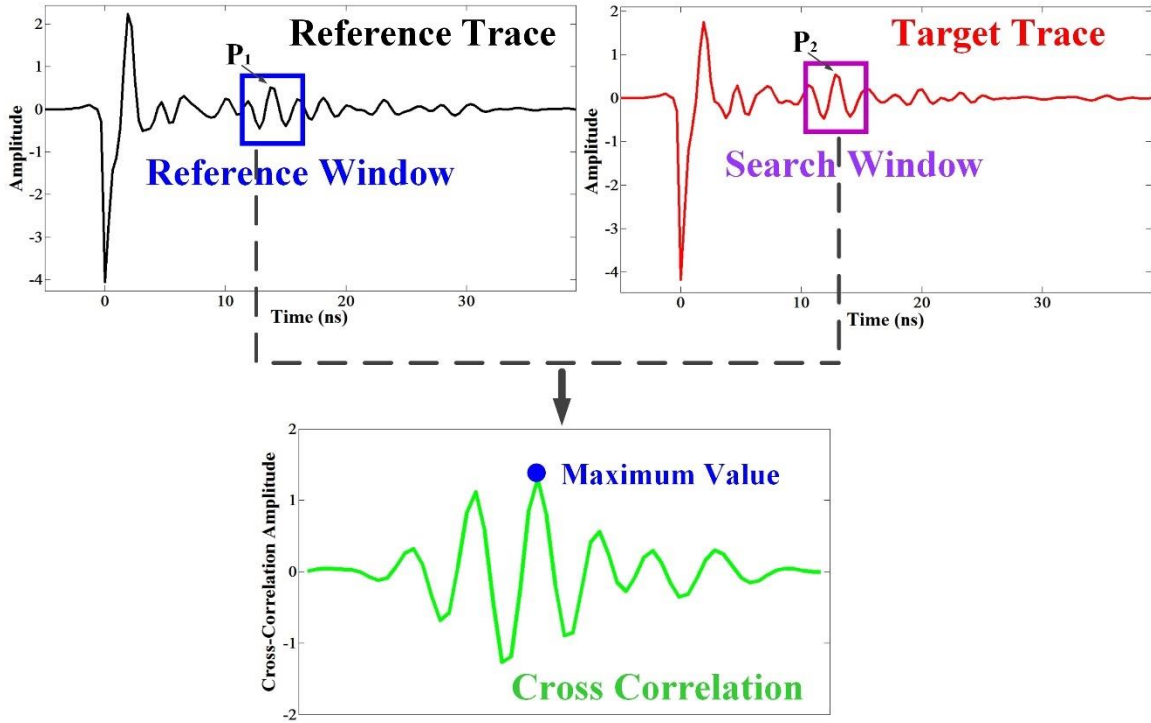


Figure S6. The schematic for the layer localization method. The black signal and red signal indicate reference trace and target trace respectively. The blue and purple rectangles indicate reference window and search window respectively. The search point is the center of both reference window and search window. The green line indicates the cross correlation between signals within reference window and search window. The blue point is maximum value of correlation.

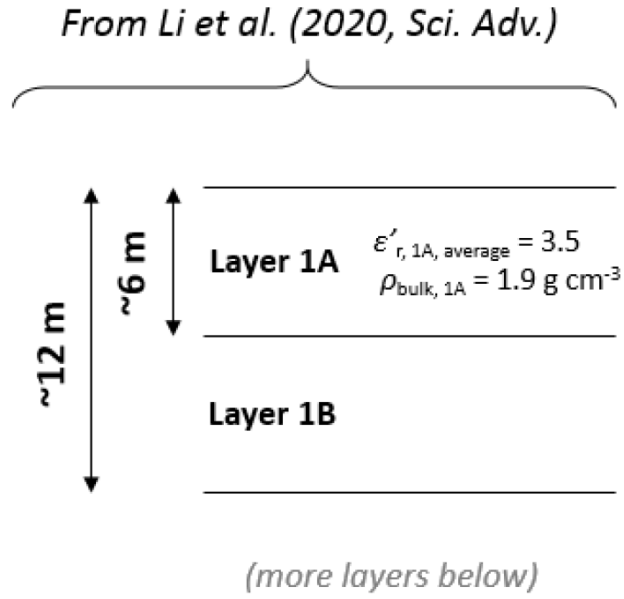


Figure S7. The model of subsurface layers in Li et al. (2020, Sci. Adv.)

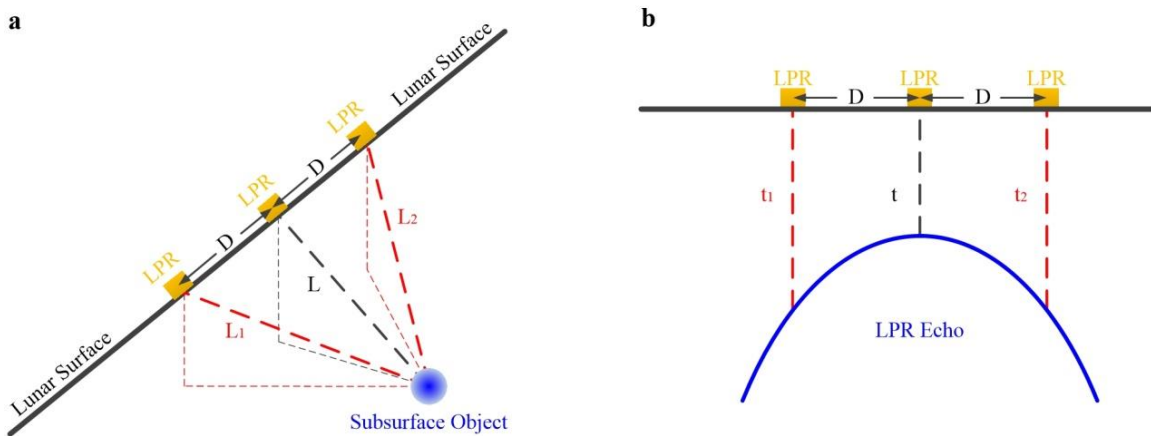


Figure S8. Mechanism of the hyperbolic fitting method.

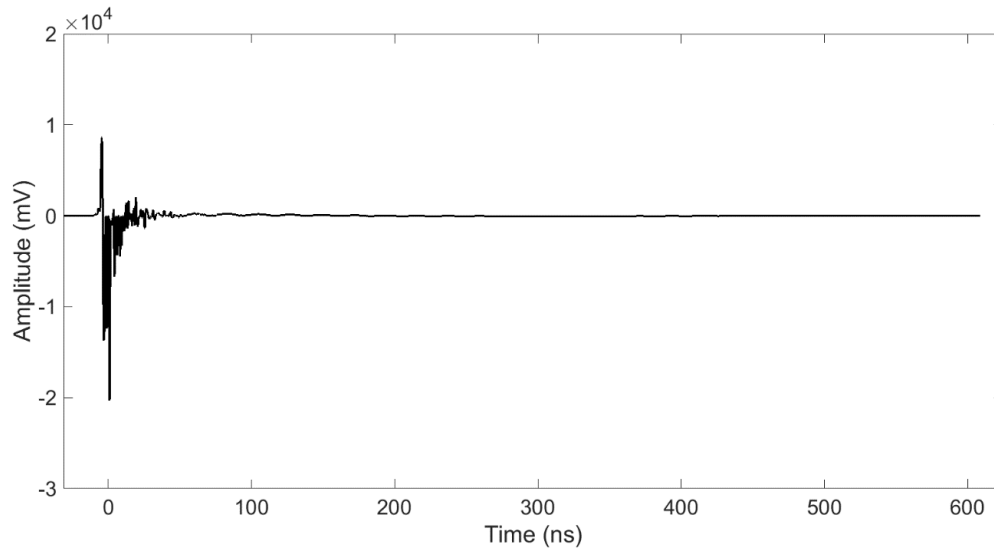


Figure S9. One trace of calibration signals of LPR Channel-II.